Three-Dimensional Extrudate Swell of Creeping Newtonian Jets

A. Karagiannis, A. N. Hrymak, J. Vlachopoulos
Department of Chemical Engineering
McMaster University
Hamilton, Ontario, CANADA L8S 4L7

The term "extrudate swell" is used to describe the increase of the diameter of a liquid jet as it emerges from an orifice, die, or duct. It is of importance in the polymer processing industry (films and pipes, coatings, profiles), since the extrusion of viscoelastic materials like polymer melts involves high extrudate swelling which may have an impact on product quality.

A large number of two-dimensional investigations of the phenomenon in exit flow out of slit and round dies are reported in the literature (Nickell et al. 1974; Crochet and Keunings, 1982; Caswell and Viriyayuthakorn, 1983; Mitsoulis et al., 1984), in which the finite element method was employed to solve the problem for Newtonian and viscoelastic fluids. Very little work has been done on the three-dimensional simulation of the phenomenon, mainly because of the complexity and size of the problem and the lack of a simple and comprehensive scheme for the free surface update during the iterative solution of the resulting nonlinear problem. The first work in the area was the boundary element prediction of the swell out of a square die by Bush and Phan-Thien (1985). More recently Trang-Cong and Phan-Thien in a series of papers applied the same approach to study the swell out of square and triangular geometries (1988a,b) and in a die-shape design problem (1988c). Shiojima and Shimazaki (1987) presented a finite element method to predict the 3-d swell out of square and rectangular dies for Newtonian and Maxwell fluids. However, neither the free surface update scheme nor any information about the swelling ratios for the studied 3-d geometries were given in this work. Trends toward three-dimensional solutions were also presented by Tanner (1986), Menges et al. (1985), and Schwenzer and Menges (1987).

The present paper deals with the three-dimensional free surface problem using the Finite Element method (Galerkin formulation). A grid generation scheme involving the simultaneous use of two different types of three-dimensional elements, brick and triangular prism elements, allowed for the simple and efficient parametrization of geometries of high complexity. This approach, in contrast to the work by Shiojima and Shimazaki (1987) and Trang-Cong and Phan-Thien (1988), does not decouple the free surface update from the velocity and pressure calculation, but it rather solves for all the unknowns simultaneously thereby taking advantage of the superior convergence properties of the Newton-Raphson scheme.

The results include the prediction of 13.5% swelling ratio for the round jet in full agreement with experimental measurements and numerical calculations (Batchelor et al., 1973; Gear et al., 1983; Tanner, 1985). The uneven swelling of rectangular dies that was observed experimentally by White and Huang (1981) was predicted for a square and a rectangular die with aspect ratio 4:1. The maximum and minimum swell ratios for the square die case were 18.41 and 2.9% for the flat face and the corner, respectively, and compared favorably with the boundary element results by Trang-Cong and Phan-Thien (1988a).

The die swell out of equilateral triangular, bow-tie- and keyhole-shaped geometries is also presented. Different swelling behavior in geometrically different regions of the same die was observed. Sharp corners may contract or exhibit little swell, while flat regions exhibit large swell. The swelling ratios depend strongly on the die geometry.

Governing Equations and Boundary Conditions

The emergence of a creeping Newtonian jet is shown schematically in Figure 1. The main flow will always be in the positive direction of the x–axis in the three-dimensional space.

The flow is incompressible, steady, creeping (zero Reynolds number), and no body forces are considered. The arbitrary shape of the die and the extrudate profile is solved in a full three-dimensional geometry.

The governing equations are the steady momentum and mass conservation equations:

$$\nabla \cdot \underline{\underline{\tau}}^* - \nabla p^* = \underline{0} \qquad (1.1\text{–}1.3)$$

$$\nabla \cdot \underline{v}^* = 0 \qquad (1.4)$$

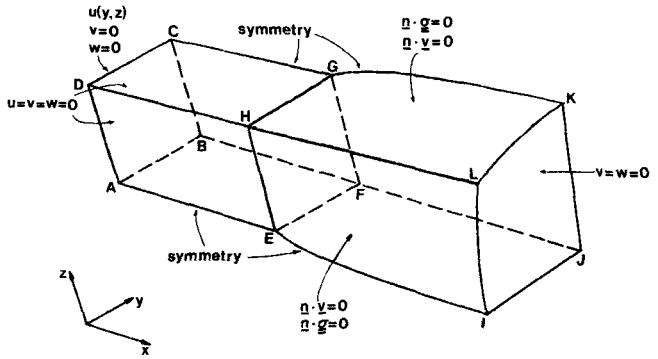

Figure 1. Emergence of a three-dimensional jet and boundary conditions.

A characteristic velocity U, length L, and viscosity μ are used to make the variables dimensionless.

The extra stress tensor $\underline{\underline{\tau}}^*$ is scaled with $\mu U/L$ and for the Newtonian case is defined as:

$$\tau_{ij}^* = \mu\left(\frac{\partial v_i^*}{\partial x_j^*} + \frac{\partial v_j^*}{\partial x_i^*}\right), \quad i,j = 1,2,3 \tag{2}$$

where μ is the Newtonian viscosity.

With respect to Figure 1, a fully developed profile is imposed upstream (plane ABCD in Figure 1), which is generated by solving the unidirectional flow problem

$$\mu\left(\frac{\partial^2 u^*}{\partial y^{*2}} + \frac{\partial^2 u^*}{\partial z^{*2}}\right) = dp^*/dx^* \quad \text{(Poisson equation)} \tag{3}$$

for the $(y - z)$ geometry of the die inlet.

The traction free boundary condition is imposed at the far downstream face (plane IJKL) where plug flow is assumed. At the die walls, the no slip boundary condition is imposed (planes DHGC and DHEA). Since no surface tension forces are considered, the extrudate surfaces (area HLKG and HLIE) are considered as force free surfaces

$$\underline{n} \cdot \underline{\underline{\sigma}}^* = \underline{0} \tag{4}$$

The free surface is a material surface with no flow through

$$\underline{n} \cdot \underline{v}^* = 0 \tag{5}$$

Symmetry conditions are imposed where possible (planes BFJKGC and AEIJFB) to reduce the size of the problem.

The set of elliptic partial differential equations (Eqs. 1) together with the boundary conditions is complete and is solved with the Galerkin/finite element method.

Two types of three-dimensional elements are used for the discretization of the flow domain into finite elements, the 27-node brick and the 18-node triangular prism element, Figure 2. Both elements are isoparametric with $C^0 - P^2$ approximation for the velocity and $C^0 - P^1$ for the pressure. We use $3 \times 3 \times 3$ integration points for the 27-node brick element and 3×7 integration points for the 18-node triangular prism element (7 points on the η, ζ triangular cross-section). For more on the shape functions and the local coordinates and weights of the integration points, refer to Dhatt and Touzot (1984).

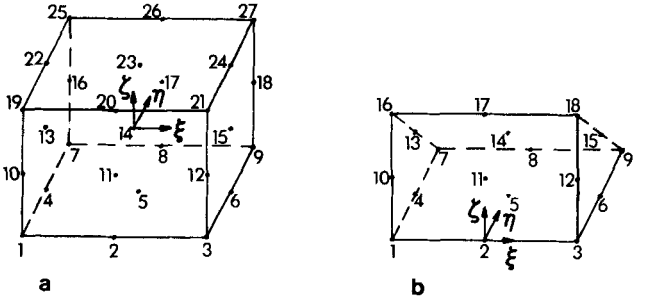

Figure 2. Parent three-dimensional elements: a) 27-node brick and b) 18-node triangular prism.

The free surface parametrization is based on the idea of spines which are predefined straight lines in space (Kistler, 1984). The free surface node $\underline{x}^i F$ is parametrized as the distance h^i along the ith spine, Figure 3. Each spine is defined by a base point $\underline{x}_0^i$ and a unit vector $\underline{e}^i$. The free surface nodes are then defined as

$$\underline{x}_F^i = \underline{x}_0^i + h^i \underline{e}^i \tag{6}$$

while the other nodes along the same spine move in constant proportions. The spines are allowed to move on a y-z plane only throughout this work.

If $\underline{x}_F^i$, $i = 1, \ldots, 9$ are the nine nodes that define a part of the free surface as the face of a 27-node brick, the free surface is

$$\underline{x} = \sum_{j=1}^{9} \underline{x}_F^j N^j(\xi, \eta = 1, \zeta) \tag{7}$$

where the 27-node element is mapped isoparametrically onto the parent ξ, η, ζ cube by the triquadratic basis functions $N^j(\xi, \eta, \zeta)$ and $\eta = 1$ the face that corresponds to the free surface.

The two types of elements are combined to simplify the grid generation and the free surface parametrization. With respect to Figure 3, where curved boundaries or corners are present, many spines originate radially from a single point toward the boundary and the 18-node elements are employed to form the first layer of elements to which layers of 27-node bricks are connected. Simple boundary shapes require only 27-node bricks.

The density of the grid along the downstream direction and the distribution of the spines have an impact on the accuracy of

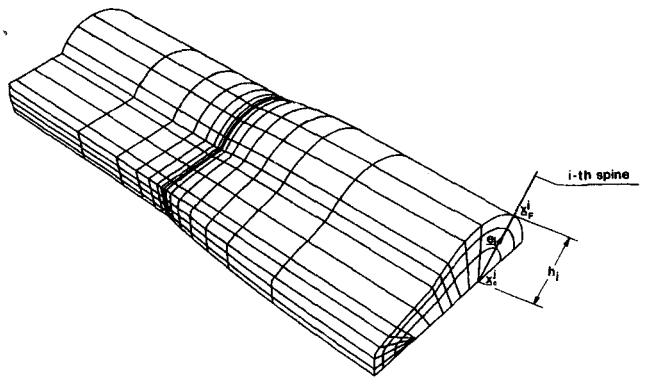

Figure 3. Perspective view of a three-dimensional finite element grid: definition of spines.

the calculated swelling ratio and on the size of the problem. The grid density along the downstream direction used in all problems dealt with in this work is shown in Figure 3 and consists of 15 "bands" of three dimensional elements. The corresponding 31 divisions are

x = 0.0, 1.0, 2.0, 2.5, 3.0, 3.25, 3.5, 3.65, 3.8, 3.9, 4.0, 4.05, 4.1, 4.125, 4.15, 4.175, 4.2, 4.25, 4.3, 4.4, 4.5, 4.65, 4.8, 5.0, 5.2, 5.45, 5.7, 6.2, 6.7, 7.7, 8.7

and the jet emerges from the $x = 4.15$ division in all cases.

Galerkin/Finite Element Formulation

The velocities and pressure are approximated within each element by:

$$v_j^{(e)} = \sum_i N^i(x, y, z) v_j^i, \qquad j = 1, 2, 3 \qquad (8.1\text{–}8.3)$$

$$p^{(e)} = \sum_i N_p^i(x, y, z) p^i \qquad (8.4)$$

where v_j^i, p^i are nodal values and N^i, N_p^i are shape functions.

The set of Eqs. 1 are discretized and the application of the standard Galerkin procedure (Huebner and Thorton, 1982) yields

$$\int_{v^{(e)}} (\nabla \cdot \underline{\underline{\sigma}}) N^i \, dV = \underline{0} \qquad (9.1\text{–}9.3)$$

$$\int_{v^{(e)}} (\nabla \cdot \underline{v}) N_p^i dV = 0 \qquad (9.4)$$

where $\underline{\underline{\sigma}} = p\underline{\underline{I}} + \underline{\underline{\tau}}$ is the total stress tensor.

After the divergence theorem is applied and the velocity components are introduced, Eqs. (9.1–9.3) with no surface traction can finally be written in the discretized form as:

$$R_x^i = \int_{-1}^{1}\int_{-1}^{1}\int_{-1}^{1} [(2\mu u_x - p)N_x^i + \mu(u_y + v_x)N_y^i + \mu(u_z + w_x)N_z^i]|J| \, d\xi \, d\eta \, d\zeta \qquad (10.1)$$

$$R_y^i = \int_{-1}^{1}\int_{-1}^{1}\int_{-1}^{1} [\mu(u_y + v_x)N_x^i + (2\mu v_y - p)N_y^i + \mu(v_z + w_y)N_z^i]|J| \, d\xi \, d\eta \, d\zeta \qquad (10.2)$$

$$R_z^i = \int_{-1}^{1}\int_{-1}^{1}\int_{-1}^{1} [\mu(u_z + w_x)N_x^i + \mu(v_z + w_y)N_y^i + (2\mu w_z - p)N_z^i]|J| \, d\xi \, d\eta \, d\zeta \qquad (10.3)$$

Equation 9.4 gives:

$$R_c^i = \int_{-1}^{1}\int_{-1}^{1}\int_{-1}^{1} (u_x + v_y + w_z)N_p^i |J| \, d\xi \, d\eta \, d\zeta \qquad (10.4)$$

while the weighted residual of the kinematic condition becomes:

$$R_k^i = \int_{-1}^{1}\int_{-1}^{1} (n_1 u + n_2 v + n_3 w)N^i |J^*| \, d\xi \, d\zeta, \quad \eta = 1 \qquad (10.5)$$

Note that only elements which have a free surface boundary contribute to the weighted kinematic residual R_k.

$|J|$ is the determinant of the Jacobian of the isoparametric transformation $(x, y, z) - (\xi, \eta, \zeta)$ where

$$\underline{\underline{J}} = \begin{Bmatrix} x_\xi & y_\xi & z_\xi \\ x_\eta & y_\eta & z_\eta \\ x_\zeta & y_\zeta & z_\zeta \end{Bmatrix} \qquad (11)$$

The vector $\underline{n}$ is the outward normal to the free surface η = constant and can be found as a vector product of any two vectors tangent to the surface. Thus

$$\underline{n} = \begin{Bmatrix} x_\xi \\ y_\xi \\ z_\xi \end{Bmatrix} \times \begin{Bmatrix} x_\zeta \\ y_\zeta \\ z_\zeta \end{Bmatrix} = \begin{Bmatrix} y_\xi & z_\zeta - y_\zeta & z_\xi \\ x_\zeta & z_\xi - x_\xi & z_\zeta \\ x_\xi & y_\zeta - x_\zeta & y_\xi \end{Bmatrix} \qquad (12)$$

$$|J^*| = \sqrt{n_1^2 + n_2^2 + n_3^2}$$

is the determinant of the Jacobian of the isoparametric transformation $(x, y, z) - (\xi, \eta = 1, \zeta)$ in the surface integral of Eq. 10.5; n_1, n_2, n_3 are the components of the normal vector to the surface $\underline{n}$.

The Galerkin/finite element procedure finally reduces the set of differential equations (Eqs. 9) into a set of algebraic equations:

$$\underline{R} = \underline{0} \qquad (13)$$

and the velocity, pressure and the free surface location can be solved for simultaneously.

Numerical Considerations

Although the constitutive equation of the Newtonian fluid is linear, the existence of a free surface renders the problem non-

Table 1. Size of the Problems

Problem	Elements	Nodes	Unknowns	Front Width	Iterations	CPUs (CRAY)**
Circular	480	3,999	11,120	522	4	680
Square	720	5,859	16,500	726	5	1,150
4:1 Rectangle	495	4,340	11,885	550	6	3,550*
Equilateral Triangle	405	3,286	9,068	443	5	387
Bow-Tie	660	5,673	15,830	701	7	1,400
Key-Hole	585	5,208	14,310	643	5	895

*CPU on the FPS-264.
**CRAY-XMP 2/2 University of Toronto Center for large-scale computation.

linear since the free surface location is not known a priori and must be solved for. An iterative scheme is required and the Newton-Raphson method is used. The full set of Eqs. 13 is solved at each iteration. Using a first-order Taylor expansion around a nominal point and assuming a relatively small change from iteration i to iteration $i+1$ in the vector of nodal variables $\underline{q} = (\underline{u}, \underline{v}, \underline{w}, \underline{p}, \underline{h})$, the Newton-Raphson iteration scheme is:

$$\underline{\underline{J}}(\underline{q}^i)\Delta\underline{q} = -\underline{R}(\underline{q}^i) \tag{14}$$

where

$$\underline{\underline{J}}(\underline{q}^i) = \frac{\partial \underline{R}}{\partial \underline{q}}\bigg|_{q_i} \tag{15}$$

$$\underline{q}^{i+1} = \underline{q}^i + \Delta\underline{q} \tag{16}$$

The Jacobian for the Newton-Raphson interations is calculated using analytical derivatives of the finite element equations.

The Newton-Raphson scheme converges with a quadratic rate of convergence normally within four to six iterations. The first iteration, with a fixed free surface, is performed to obtain initial estimates of the velocities and pressure and does not enter the iteration count. The initial shape of the free surface is given as that of the die exit in all problems. The method is relatively robust since convergence was always attained for the problems investigated but fewer iterations may have been needed if a better estimate of the extrudate shape was supplied. The termination criterion is that the maximum relative update be less than 10^{-6}.

The resulting system of simultaneous equations at each iteration was on the order of 8,000–17,000 equations and was solved with a frontal solver by Taylor and Hughes (1981). Frontwidths were on the order of 400–750 and depend on the $(y-z)$ density of the grid.

The development of the computer code was done on a VAX 8600 but the runs were done on the CRAY-XMP 2/2 at the University of Toronto and the FPS-264 at McMaster University.

Details on the size of the problems with respect to the number of elements, number of nodes, number of variables and the total CPU times are given in Table 1. The use of a highly vectorized solver may lead to significant reduction of the CPU time requirement since over 70% of the total CPU time is spent in the frontal solver routine for all the problems dealt with.

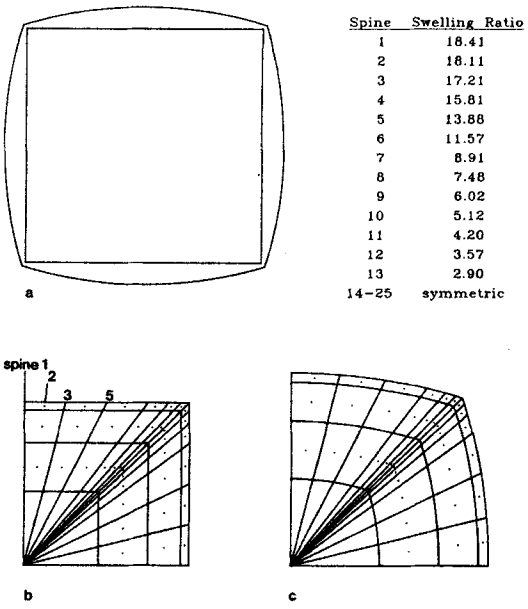

Figure 5. Extrudate swell from a square die: a) superposed die shape and final shape of the extrudate; b) initial grid; and c) final grid.

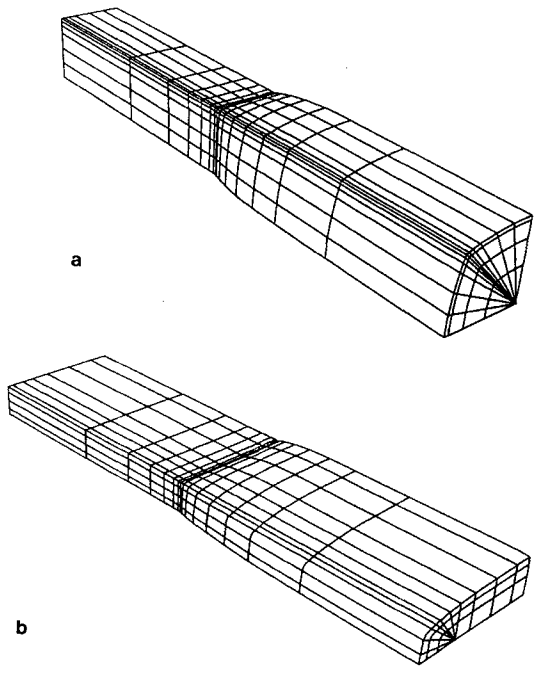

Figure 4. Perspective view of the three-dimensional extrudate swell from a) square die and b) rectangular die of aspect ratio 4:1.

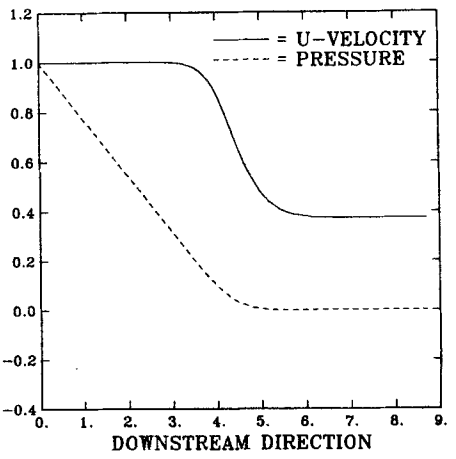

Figure 6. Extrudate swell from a square die: normalized downstream velocity and pressure distribution along the centerline.

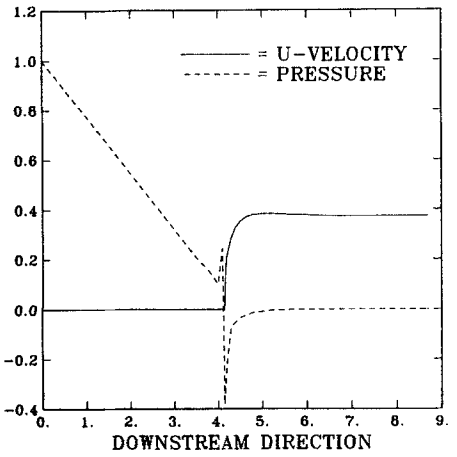

Figure 7. Extrudate swell from a square die: normalized downstream velocity and pressure distribution along the center of the flat face (scale the same as in Figure 7).

Results and Discussion

As a test of the numerical method, we consider a Newtonian creeping jet emerging from a cylindrical die. The problem is solved as fully three dimensional and the calculated swelling ratio of 13.5% is in full agreement with corresponding experimental and theoretical evidence (Batchelor et al., 1973; Gear et al., 1983; Tanner, 1985).

Because of the nonexistence of a profound reference point in some die shapes (e.g., key-hole die) the swelling ratio is always defined as

$$\text{swelling ratio} = (h^i_{\text{final}} - h^i_{\text{initial}})/(h^i_{\text{initial}})$$

along the ith spine.

The extrusion of a Newtonian fluid from a square die was investigated. Due to symmetry one quarter of the flow domain is considered and a perspective view of the final three dimensional grid is shown in Figure 4a. The material exhibits a maximum swell of 18.41% at the planes of symmetry and a minimum swell of 2.9% at the corner, Figure 5. These results were predicted for a mesh of 720 elements, 5,859 nodes and 16,500 unknowns. For a less dense mesh of 480 elements, 3,999 nodes and 11,120 unknowns, a maximum swell of 18.9% and a minimum swell of 2.99% are predicted which are within 3% of the more dense grid predictions. The boundary element study by Tran-Cong and Phan-Thien 1988, predicts a lower swell (18% compared to 18.4%) at the flat regions but a higher swell (3.4% compared to 2.9%) at the corners.

The pressure and downstream velocity distribution is shown in Figures 6–8 along the centerline, along the center of the face (symmetry plane) and along the corner points for the square die problem. No acceleration of the centerline fluid is predicted, Figure 6, in contrast to the prediction of Bush and Phan-Thien (1985). The fluid at the centerline flows with constant velocity

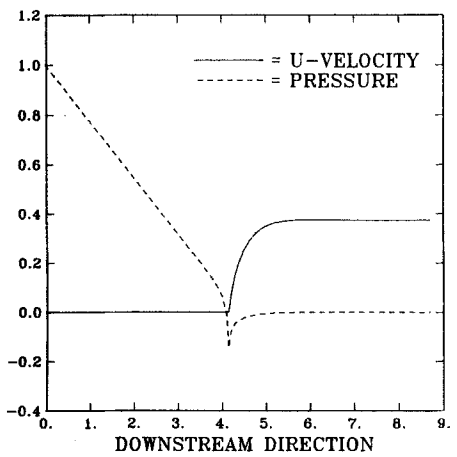

Figure 8. Extrudate swell from a square die: normalized downstream velocity and pressure distribution along the corner points (scale the same as in Figure 7).

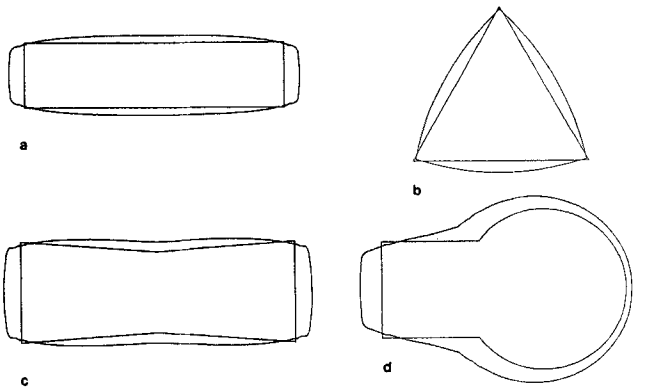

Figure 9. Superposed die shape and final shape of the extrudate of: a) rectangualr die of aspect ratio 4:1; b) equilateral triangular die; c) bow-tie die; and d) key-hole shaped die.

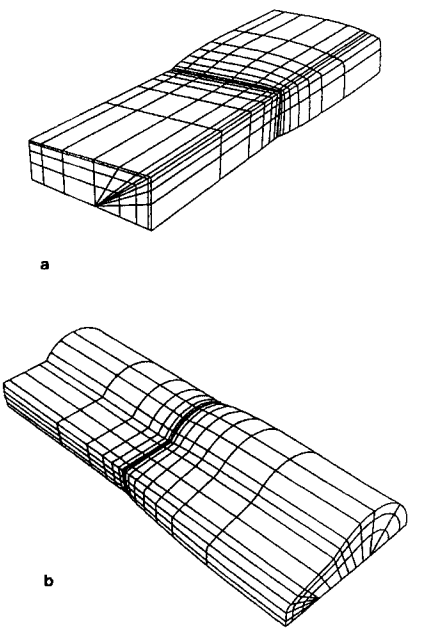

Figure 10. Perspective view of the three dimensional extrudate swell from a) bow-tie die and b) key-hole shaped die.

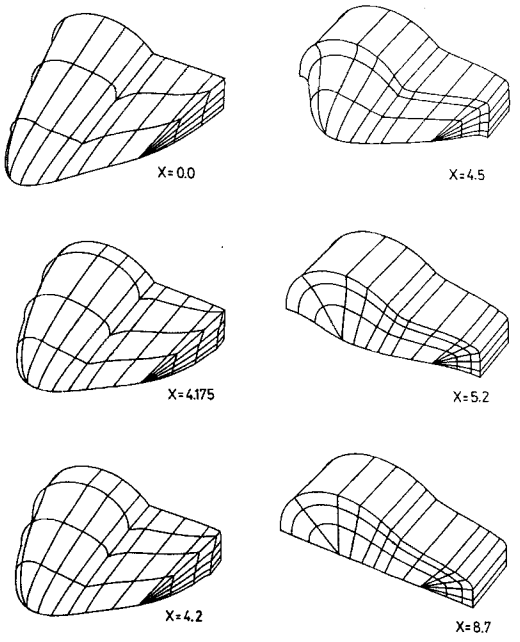

Figure 11. Three-dimensional view of the downstream component of velocity; key-hole shaped die. Die exit at $x = 4.15$.

in the region of fully developed flow until it reaches the region of the die exit and then it monotonically decelerates to the plug flow value. The pressure distribution along the center of the face exhibits the well known (Caswell and Viriyayuthakorn, 1983; Mitsoulis et al., 1984) behavior of the corresponding two dimensional solution of the swell from a slit, Figure 7. The pressure exhibits a discontinuous increase before the exit of the die where it takes negative value while the pressure distribution along the corner points, Figure 8, does not exhibit this increase but rather drops smoothly to a negative value probably because of the force balance in that region. The same behavior of the pressure discontinuity was observed in all the problems where a sharp corner was present.

The large size of the problems and the prohibitively high computer costs forced the use of less dense grids in the $(y - z)$ plane as a compromise between economy and accuracy for the other problems investigated.

It is interesting that when the extrudate swell from a rectangular die of aspect ratio 4:1 is considered, Figures 4b and 9a, the material actually contracts at the corners while it exhibits large swell at the symmetry planes. In this case the material at the corner is pushed inward to keep the force balance as the flow field changes. The distorted free surface shape is attributed to the C° approximation of the free surface (slope is not continuous across interelement boundaries).

The equilateral triangular geometry was also considered and a slight contraction of 2.6% was observed at the corners in the final shape, Figure 9b, while the maximum swell of 22.8% occurs at the flat face. The corresponding results of Tran-Cong and Phan-Thien (1988) were 2% contraction at the corner and 20.6% swell at the flat face. As was also the case with the square geometry, it seems that the boundary element method predicts lower swelling ratios at the flat faces but higher at the corners compared to the finite element results.

Another interesting die geometry which finds use in the polymer processing industry to counter-balance the swell that is observed at the flat faces of the rectangular dies, is the bow-tie shaped geometry, Figures 9c and 10a. The width of the die at the neck is taken arbitrarily as 80% of the maximum width and the final shape of the extrudate in this case is approaching the rectangular shape, Figure 9c.

Finally, the extrudate swell problem from a key-hole shaped die was examined, Figures 9d and 10b. This geometry is the most complicated since it comprises one round and one rectangular part and therefore possesses different flow characteristics in each part. The final shape of the extrudate is complicated and very uneven, Figure 9d. The swelling is more pronounced near the region of transition from one geometry to the other and also at the far end of the rectangular section.

In Figure 11, three-dimensional plots of the downstream component of velocity are shown in different stations downstream. The fluid in the round part is moving faster than in the rectangular section initially, but as the jet emerges out of the die and expands, it gradually decelerates while the fluid in the rectangular section accelerates and finally plug flow is attained far downstream.

Acknowledgments

Financial assistance from the Natural Sciences and Engineering Research Council of Canada is gratefully acknowledged. A. Karagiannis was also the recipient of a Shell Canada Graduate Research Fellowship. We also thank NSERC and the Center for Large Scale Computation of the University of Toronto for computer time on the CRAY X-MP 2/2.

The authors wish to thank the reviewers for bringing the recent papers of Shiojima and Shimazaki, and Tran-Cong and Phan-Thien to our attention.

Notation

$\underline{e}$ = unit vector
$\bar{h}$ = free surface position parameter
I = unit tensor
J = Jacobian matrix
L = characteristic length scale
$\underline{n}$ = outward unit normal vector
n_1, n_2, n_3 = components of the outward unit normal vector
N = velocity basis function
N_p = pressure basis function
p = pressure
$\underline{q}$ = vector of unknowns
$\underline{R}$ = vector of residuals
R_x, R_y, R_z = x-, y-, z-momentum residual
R_c = continuity residual
R_k = kinematic residual
u, v, w = x-, y-, z-component of velocity
U = characteristic velocity scale
$\underline{v}$ = velocity vector
x, y, z = global coordinates

Greek letters

ξ, η, ζ = local coordinates
μ = viscosity
$\underline{\underline{\sigma}}$ = total stress tensor
$\underline{\underline{\tau}}$ = extra stress tensor

Superscripts

(e) = of element
i = quantity associated with the ith node or spine
$*$ = dimensional quantity

Subscripts

F = free surface
o = base point
x, y, z = differentiation *w.r.t.* x, y, z
ξ, η, ζ = differentiation *w.r.t.* ξ, η, ζ

Literature Cited

Batchelor, J., J. P. Berry, and F. Horsfall, "Die Swell in Elastic and Viscous Fluids," *Pol.*, **14**, 297 (1973).

Bush, M. B., and N. Phan-Thien, "Three Dimensional Viscous Flows with a Free Surface: Flow out of Long Square Die," *J. Non-Newtonian Fluid Mech.*, **18**, 211 (1985).

Caswell, B., and M. Viriyayuthakorn, "Finite Element Simulation of Die Swell for a Maxwell Fluid," *J. Non-Newtonian Fluid Mech.*, **12**, 13 (1983).

Dhatt, G., and G. Touzot, *The Finite Element Method Displayed*, Wiley, New York (1984).

Crochet, M. J., and R. Keunings, "On Numerical Die Swell Calculation," *J. Non-Newtonian Fluid Mech.*, **10**, 85 (1982).

Gear, R. L., M. Keentok, J. F. Milthorpe and R. I. Tanner, "The Shape of Low Reynolds Number Jets," *Phys. Fluids*, **26**, 7 (1983).

Huebner, K. H., and E. A. Thornton, *The Finite Element Method for Engineers*, 2nd ed., Wiley, New York (1982).

Kistler, S. F., "The Fluid Mechanics of Curtain Coating and Related Viscous Free Surface Flows with Contact Lines," Ph.D. Thesis, Univ. of Minnesota, Minneapolis (1984).

Menges, G., B. Gesenhues, and C. Schwenzer, "A Method of Calculating Die Swell when Designing Profile Dies," *Kunststoffe*, **75**, 14 (1985).

Mitsoulis, E., J. Vlachopoulos, and F. A. Mirza, "Simulation of Extrudate Swell from Long Slit and Capillary Dies," *Pol. Proc. Eng.*, **2**, 153 (1984).

Nickell, R. E., R. I. Tanner, and B. Caswell, "The Solution of Viscous Incompressible Jet and Free-Surface Flows using Finite-Element Methods," *J. Fluid Mech.*, **65**, 189 (1974).

Schwenzer, C., and G. Menges, "Megapus—A Program-Package for the Layout of Extrusion Lines," *Proc. ANTEC'87* Conf., Los Angeles, 109 (1987).

Shiojima, T., and Y. Shimazaki, "Three-Dimensional Finite Element Analyses for a Maxwell Fluid Using the Penalty Function Method," *Proc. NUMETA '87*, Swansea, G. N. Pande, and J. Middleton, eds. (1987).

Tanner, R. I., *Engineering Rheology*, Clarendon Press, Oxford (1985).

———, "The Computer Simulation of Plastics Extrusion," *Proc. NUMIFORM* Conf., Gothenburg (1986).

Taylor, C., and T. G. Hughes, *Finite Element Programming of the Navier-Stokes Equations*, Pineridge Press Ltd, Swansea (1981).

Tran-Cong, T., and N. Phan-Thien, "Three-Dimensional Extrusion Processes by Boundary Element Method: 1. An Implementation of High-Order Elements and Some Newtonian Results," *Rheol. Acta*, **27**, 21 (1988a).

———, "Three-Dimensional Extrusion Processes by Boundary Element Method: 2. Extrusion of a Visoelastic Fluid," *Rheol. Acta*, submitted (1988b).

———, "Die Design by a Boundary Element Method," *J. Non-Newtonian Fluid Mech.*, submitted (1988c).

White, J. L., and D. Huang, "Extrudate Swell and Extrusion Pressure Loss of Polymer Melts Flowing through Rectangular and Trapezoidal Dies," *Pol. Eng. Sci.*, **21**, 1101 (1981).

Manuscript received Jan. 28, 1988, and revision received June 23, 1988.